

Change-over switch for quantum states transfer with topological channels in a circuit-QED lattice

Liu-Yong Cheng(程留永), Li-Na Zheng(郑黎娜), Ruixiang Wu(吴瑞祥), Hong-Fu Wang(王洪福), and Shou Zhang(张寿)

Citation: Chin. Phys. B, 2022, 31 (**2**): 020305. DOI: 10.1088/1674-1056/ac2f2e
Journal homepage: http://cpb.iphy.ac.cn; http://iopscience.iop.org/cpb

What follows is a list of articles you may be interested in

Topology of a parity-time symmetric non-Hermitian rhombic lattice

Shumai Zhang(张舒迈), Liang Jin(金亮), and Zhi Song(宋智)
Chin. Phys. B, 2022, 31 (**1**): 010312. DOI: 10.1088/1674-1056/ac364a

Efficient and stable wireless power transfer based on the non-Hermitian physics

Chao Zeng(曾超), Zhiwei Guo(郭志伟), Kejia Zhu(祝可嘉), Caifu Fan(范才富), Guo Li(李果), Jun Jiang(江俊), Yunhui Li(李云辉), Haitao Jiang(江海涛), Yaping Yang(羊亚平), Yong Sun(孙勇), and Hong Chen(陈鸿)
Chin. Phys. B, 2022, 31 (**1**): 010307. DOI: 10.1088/1674-1056/ac3815

High winding number of topological phase in non-unitary periodic quantum walk

Yali Jia(贾雅利) and Zhi-Jian Li(李志坚)
Chin. Phys. B, 2021, 30 (**10**): 100301. DOI: 10.1088/1674-1056/abf554

Superfluid states in α-T_3 lattice

Yu-Rong Wu(吴玉容) and Yi-Cai Zhang(张义财)
Chin. Phys. B, 2021, 30 (**6**): 060306. DOI: 10.1088/1674-1056/abea8a

Realization of arbitrary two-qubit quantum gates based on chiral Majorana fermions

Qing Yan(闫青) and Qing-Feng Sun(孙庆丰)
Chin. Phys. B, 2021, 30 (**4**): 040303. DOI: 10.1088/1674-1056/abe296

Change-over switch for quantum states transfer with topological channels in a circuit-QED lattice

Liu-Yong Cheng(程留永)[1,2,†], Li-Na Zheng(郑黎娜)[1], Ruixiang Wu(吴瑞祥)[1,2], Hong-Fu Wang(王洪福)[3], and Shou Zhang(张寿)[3]

[1] *School of Physics and Information Engineering, Shanxi Normal University, Linfen* 041004, *China*
[2] *Key Laboratory of Spectral Measurement and Analysis of Shanxi Province, Shanxi Normal University, Linfen* 041004, *China*
[3] *Department of Physics, College of Science, Yanbian University, Yanji* 133002, *China*

(Received 27 August 2021; revised manuscript received 23 September 2021; accepted manuscript online 13 October 2021)

We propose schemes to realize robust quantum states transfer between distant resonators using the topological edge states of a one-dimensional circuit quantum electrodynamics (QED) lattice. Analyses show that the distribution of edge states can be regulated accordingly with the on-site defects added on the resonators. And we can achieve different types of quantum state transfer without adjusting the number of lattices. Numerical simulations demonstrate that the on-site defects can be used as a change-over switch for high-fidelity single-qubit and two-qubit quantum states transfer. This work provides a viable prospect for flexible quantum state transfer in solid-state topological quantum system.

Keywords: quantum states transfer, edge states, change-over switch, circuit quantum electrodynamics (QED) lattice

PACS: 03.67.–a, 42.50.Pq **DOI:** 10.1088/1674-1056/ac2f2e

1. Introduction

Quantum state transfer (QST) between distant nodes is at the heart of quantum information processing and quantum networking.[1–7] Over the past decades, a variety of theoretical and experimental schemes for states transfer have been proposed in different quantum systems.[8–20] Secure and efficient quantum information process usually needs high-fidelity QST, which raises a higher demand to physical systems and operations. Compared with other platforms, the circuit quantum electrodynamics (QED) has attracted substantial attention because of its operability,[21,22] readability, ready fabrication,[23] etc.[24–26] Although the circuit-QED system has many advantages for quantum information processing and quantum computing, the inevitable existence of disorder and disturbance still lead to the decoherence effect of the practical system.

Topological insulators[27–32] are electronic materials, which have a bulk band gap like ordinary insulators but have protected conducting states on their boundaries or surfaces. These conducting edge states are immune to the local disorders and perturbations because of the protection originating from the topological structure of the energy bands.[29,33–37] This makes the topological insulators have many potential applications in quantum information field,[38–46] such as robust QST[38,40,45,46] and topological quantum computing. Mei *et al.*[38] presented experimentally feasible schemes for realizing robust QST via topologically protected edge states in superconducting qubit chains. Their work studied transfer schemes of single-qubit states and two-qubit entangled states via the topological edge states in different types of qubit chains. Lemonde *et al.*[46] analyzed the robust acoustic edge states in a two-dimension optomechanical array and realized a state transfer protocol between spin qubits located in distant cavities. However, among various topological systems, the on-site defect is often regarded as a negative factor in the quantum information process. A recent paper[47] researched a switch mechanism of robust QST channel by appropriately introducing the on-site defect on a flux qubit chain. Under the mechanism in Ref. [47], robust single-qubit quantum information transmission or storage can be effectively controlled.

In this paper, we investigate two types of QST with different topologically protected channels in a single one-dimensional circuit-QED lattice. By modulating the photon hopping rates and the resonator frequency shift, the one-dimensional circuit-QED lattice can be remodeled as a generalized Su–Schrieffer–Heeger (SSH) model, which possesses various topological phases. Then the theoretical analyses exhibit that the transfer of two-qubit quantum state can be realized by using the edge states of the lattice. Subsequent numerical simulation results show high fidelity of QST with the adiabatic evolution conditions. More importantly, via adding on-site defects to different resonators, we find that the distribution of these topological edge states changes accordingly. The changed-edge states can be used as new topologically protected quantum channels to realize robust QST of single-qubit and two-qubit quantum states. We demonstrate that the on-site defects can play the role of change-over switch and steer the lattice into a multifunctional transfer channel with a one-dimensional circuit-QED system.

[†]Corresponding author. E-mail: lycheng@sxnu.edu.cn

© 2022 Chinese Physical Society and IOP Publishing Ltd

2. System and generalized SSH model

The physical system to consider here is a one-dimensional circuit-QED lattice with N unit cells, as shown in Fig. 1. The transmission line resonators (TLR) labeled a_n, b_n, c_n form a unit cell, while the N-th unit cell possesses a_N and b_N without c_N. The resonators a_n and b_n possess indirect neighbor interactions. They are both coupled to a tunable superconducting qubit $Q_{1,n}$, while b_n and c_n couple with each other via the superconducting qubit $Q_{2,n}$. a_{n+1} and c_n that belong to two adjacent unit cells are coupled to the qubit $Q_{3,n}$. Meanwhile, the tunable superconducting qubits $Q_{a,n}$, $Q_{b,n}$ and $Q_{c,n}$ are embedded inside three resonators a_n, b_n and c_n successively to provide additional control over the frequency shift of the resonator modes with coupling strengths g_a, g_b and g_c. The entire system can be dominated by the Hamiltonian ($\hbar = 1$)

$$H_{\rm tot} = H_{\rm free} + H_{R-q} + H_{\rm hopping}. \tag{1}$$

where $H_{\rm free}$ is the free Hamiltonian of TLR and superconducting qubits, which can be modeled as

$$\begin{aligned} H_{\rm free} = \sum_n \Big[& \omega_{a,n} a_n^\dagger a_n + \omega_{b,n} b_n^\dagger b_n + \omega_{c,n} c_n^\dagger c_n \\ & + \frac{\omega_{q1,n}}{2}\sigma_{q1,n}^z + \frac{\omega_{q2,n}}{2}\sigma_{q2,n}^z + \frac{\omega_{q3,n}}{2}\sigma_{q3,n}^z \\ & + \frac{\omega_{qa,n}}{2}\sigma_{qa,n}^z + \frac{\omega_{qb,n}}{2}\sigma_{qb,n}^z + \frac{\omega_{qc,n}}{2}\sigma_{qc,n}^z \Big]. \end{aligned} \tag{2}$$

Here, $\omega_{i,n}$ $(i = a,b,c)$ and $\omega_{qj,n}$ $(j = a,b,c,1,2,3)$ are the frequencies of the TLR and the superconducting qubit. The collective coupling between resonators and the embedded qubits can be defined as

$$H_{R-q} = \sum_n [g_a \sigma_{qa,n}^\dagger a_n + g_b \sigma_{qb,n}^\dagger b_n + g_c \sigma_{qc,n}^\dagger c_n + {\rm H.c.}]. \tag{3}$$

In addition, the last term of Eq. (1) represents the interaction between resonators and two adjacent qubits with coupling strength g_j,

$$H_{\rm hopping} = \sum_n [g_1 \sigma_{q1,n}^\dagger a_n + g_1 \sigma_{q1,n}^\dagger b_n + g_2 \sigma_{q2,n}^\dagger b_n + g_2 \sigma_{q2,n}^\dagger c_n + g_3 \sigma_{q3,n}^\dagger a_{n+1} + g_3 \sigma_{q3,n}^\dagger c_n + {\rm H.c.}]. \tag{4}$$

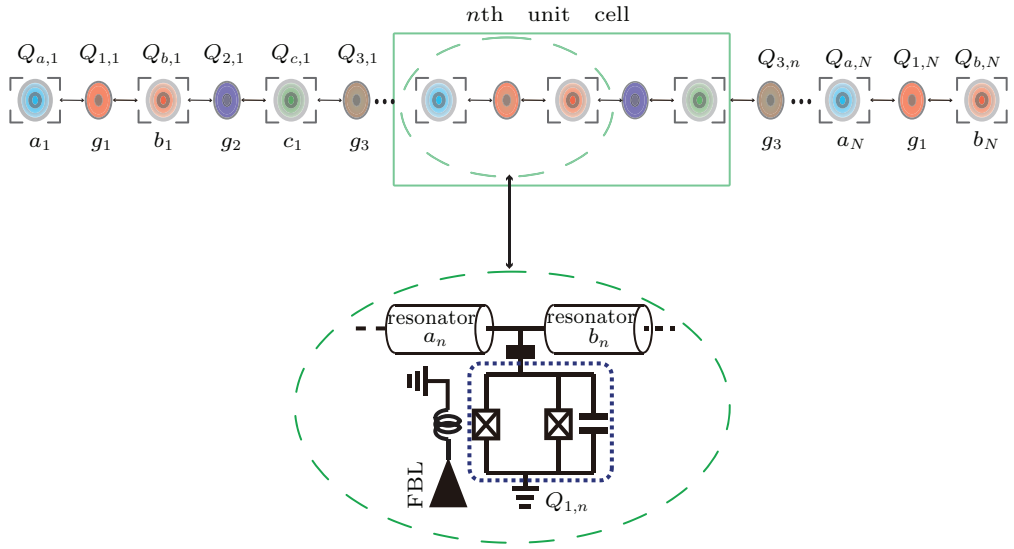


Fig. 1. Schematic of 1D circuit-QED lattice. Each unit cell (the rectangle) of the lattice contains three resonators labeled as a_n, b_n and c_n. Resonators a_n, b_n and c_n contain three superconducting qubits $Q_{a,n}$, $Q_{b,n}$ and $Q_{c,n}$, respectively, accompanying with the coupling strengths g_a, g_b and g_c. Two nearest-neighbor resonators a_n (b_n) and b_n (c_n) in one unit cell couple with each other via an assisted superconducting qubit $Q_{1,n}$ ($Q_{2,n}$) with the coupling strength g_1 (g_2). While two resonators c_n and a_{n+1} belonging to two unit cells couple with each other via a qubit $Q_{3,n}$ with the coupling strength g_3. The dashed circle represents the circuit diagram of the coupling between two indirect adjacent resonators via a superconducting qubit. The energy level space of each qubit can be tuned via magnetic flux provided by a flux-bias line (FBL).

In the rotating frame with respect to the external driving frequency $\omega_{\rm d}$ and in the interaction picture with respect to the superconducting qubits frequencies $\omega_{qj,n}$, the Hamiltonian becomes

$$H'_{\rm free} = \sum_n [\Delta_{a,n} a_n^\dagger a_n + \Delta_{b,n} b_n^\dagger b_n + \Delta_{c,n} c_n^\dagger c_n],$$

$$\begin{aligned} H'_{R-q} = \sum_n \Big[& \frac{g_a^2}{\Delta_{qa,n}} (|e\rangle_{qa,n}\langle e| a_n a_n^\dagger - |g\rangle_{qa,n}\langle g| a_n^\dagger a_n) + \frac{g_b^2}{\Delta_{qb,n}} (|e\rangle_{qb,n}\langle e| b_n b_n^\dagger - |g\rangle_{qb,n}\langle g| b_n^\dagger b_n) \\ & + \frac{g_c^2}{\Delta_{qc,n}} (|e\rangle_{qc,n}\langle e| c_n c_n^\dagger - |g\rangle_{qc,n}\langle g| c_n^\dagger c_n) \Big], \end{aligned}$$

$$
\begin{aligned}
H'_{\text{hopping}} = & \sum_n \frac{g_1^2}{\Delta_{q1,n}}[(|e\rangle_{q1,n}\langle e|a_n a_n^\dagger - |g\rangle_{q1,n}\langle g|a_n^\dagger a_n) + (|e\rangle_{q1,n}\langle e|b_n b_n^\dagger - |g\rangle_{q1,n}\langle g|b_n^\dagger b_n)] \\
& + \frac{g_2^2}{\Delta_{q2,n}}[(|e\rangle_{q2,n}\langle e|b_n b_n^\dagger - |g\rangle_{q2,n}\langle g|b_n^\dagger b_n) + (|e\rangle_{q2,n}\langle e|c_n c_n^\dagger - |g\rangle_{q2,n}\langle g|c_n^\dagger c_n)] \\
& + \frac{g_3^2}{\Delta_{q3,n}}[(|e\rangle_{q3,n}\langle e|a_{n+1} a_{n+1}^\dagger - |g\rangle_{q3,n}\langle g|a_{n+1}^\dagger a_{n+1}) + (|e\rangle_{q3,n}\langle e|c_n c_n^\dagger - |g\rangle_{q3,n}\langle g|c_n^\dagger c_n)] \\
& + \Bigg[\frac{g_1^2}{\Delta_{q1,n}}(|e\rangle_{q1,n}\langle e|a_n b_n^\dagger - |g\rangle_{q1,n}\langle g|b_n^\dagger a_n) + \frac{g_2^2}{\Delta_{q2,n}}(|e\rangle_{q2,n}\langle e|b_n c_n^\dagger - |g\rangle_{q2,n}\langle g|c_n^\dagger b_n) \\
& + \frac{g_3^2}{\Delta_{q3,n}}(|e\rangle_{q3,n}\langle e|a_{n+1} c_n^\dagger - |g\rangle_{q3,n}\langle g|c_n^\dagger a_{n+1}) + \text{H.c.}\Bigg]. \qquad (5)
\end{aligned}
$$

Here $\Delta_{i,n} = \omega_{i,n} - \omega_{\text{d}}$ is the detuning between the resonator and external driving field, $\Delta_{qj,n} = \omega_{qj,n} - \omega_{\text{d}}$ represents the detuning of the qubits. Under the dispersive regime,[48] if all qubits are prepared in the ground state, the coupling between the qubit and the resonator is removed. After that, the total Hamiltonian can be rewritten as

$$
\begin{aligned}
H_{\text{eff}}^0 = & \sum_n \left(\Delta_{a,n} - \frac{g_1^2}{\Delta_{q1,n}} - \frac{g_a^2}{\Delta_{qa,n}} - \frac{g_3^2}{\Delta_{q3,n}}\right) a_n^\dagger a_n \\
& + \left(\Delta_{b,n} - \frac{g_1^2}{\Delta_{q1,n}} - \frac{g_b^2}{\Delta_{qb,n}} - \frac{g_2^2}{\Delta_{q2,n}}\right) b_n^\dagger b_n \\
& + \left(\Delta_{c,n} - \frac{g_2^2}{\Delta_{q2,n}} - \frac{g_c^2}{\Delta_{qc,n}} - \frac{g_3^2}{\Delta_{q3,n}}\right) c_n^\dagger c_n \\
& + \Bigg[-\frac{g_1^2}{\Delta_{q1,n}} b_n^\dagger a_n - \frac{g_2^2}{\Delta_{q2,n}} c_n^\dagger b_n \\
& - \frac{g_3^2}{\Delta_{q3,n}} a_{n+1}^\dagger c_n + \text{H.c.}\Bigg]. \qquad (6)
\end{aligned}
$$

The first three terms denote the on-site energy of the resonators with qubit-induced resonator frequency shift, the remaining terms represent the coupling between two nearest-neighbor resonators assisted by the qubit-mediated photon hopping.[48] Resetting the energy zero point with respect to the resonator detuning ($\omega_{i,n} - \omega_{\text{d}} = 0$), Eq. (6) can be described as

$$
\begin{aligned}
H_{\text{eff}}^1 = & \sum_n -\left(\frac{g_1^2}{\Delta_{q1,n}} + \frac{g_a^2}{\Delta_{qa,n}} + \frac{g_3^2}{\Delta_{q3,n}}\right) a_n^\dagger a_n \\
& - \left(\frac{g_1^2}{\Delta_{q1,n}} + \frac{g_b^2}{\Delta_{qb,n}} + \frac{g_2^2}{\Delta_{q2,n}}\right) b_n^\dagger b_n \\
& - \left(\frac{g_2^2}{\Delta_{q2,n}} + \frac{g_c^2}{\Delta_{qc,n}} + \frac{g_3^2}{\Delta_{q3,n}}\right) c_n^\dagger c_n \\
& - \Bigg[\frac{g_1^2}{\Delta_{q1,n}} b_n^\dagger a_n + \frac{g_2^2}{\Delta_{q2,n}} c_n^\dagger b_n \\
& + \frac{g_3^2}{\Delta_{q3,n}} a_{n+1}^\dagger c_n + \text{H.c.}\Bigg], \qquad (7)
\end{aligned}
$$

where $\Delta_{qj,n} = \omega_{qj,n} - \omega_{\text{d}}$ ($j = 1,2,3,a,b,c$) also can be described as $\Delta_{qj,n} = \omega_{qj,n} - \omega_{i,n}$. As we can see, the photon hopping rates and the resonator frequency shift could be directly tuned by changing the qubit detuning $\Delta_{qj,n}$ via external control circuits to adjust the qubit frequency $\omega_{qj,n}$. Based on this advantage, each of the coefficients in Eq. (7) becomes modulated. In order to construct a generalized SSH Hamiltonian, we focus on lattice Hamiltonian Eq. (7) confined to the following parameter conditions:

$$
\begin{aligned}
J_1 &= -\frac{g_1^2}{\Delta_{q1,n}} = \cos\left(\frac{2\pi}{3} + \theta\right), \\
J_2 &= -\frac{g_2^2}{\Delta_{q2,n}} = \cos\left(\frac{4\pi}{3} + \theta\right), \\
J_3 &= -\frac{g_3^2}{\Delta_{q3,n}} = \cos\left(\frac{6\pi}{3} + \theta\right), \\
&\frac{g_1^2}{\Delta_{q1,n}} + \frac{g_a^2}{\Delta_{qa,n}} + \frac{g_3^2}{\Delta_{q3,n}} = 0, \\
&\frac{g_1^2}{\Delta_{q1,n}} + \frac{g_b^2}{\Delta_{qb,n}} + \frac{g_2^2}{\Delta_{q2,n}} = 0, \\
&\frac{g_2^2}{\Delta_{q2,n}} + \frac{g_c^2}{\Delta_{qc,n}} + \frac{g_3^2}{\Delta_{q3,n}} = 0, \qquad (8)
\end{aligned}
$$

where the parameters θ can be tuned from 0 to 2π. The conditions described in Eq. (8) can be realized by externally tuning the superconducting frequencies as

$$
\begin{aligned}
\omega_{q1,n} &= \omega_{i,n} - g_1^2 / \cos\left(\frac{2\pi}{3} + \theta\right), \\
\omega_{q2,n} &= \omega_{i,n} - g_2^2 / \cos\left(\frac{4\pi}{3} + \theta\right), \\
\omega_{q3,n} &= \omega_{i,n} - g_3^2 / \cos\left(\frac{6\pi}{3} + \theta\right), \\
\omega_{qa,n} &= \omega_{i,n} + g_a^2 \Big/ \left[\cos\left(\frac{2\pi}{3} + \theta\right) + \cos\left(\frac{6\pi}{3} + \theta\right)\right], \\
\omega_{qb,n} &= \omega_{i,n} + g_b^2 \Big/ \left[\cos\left(\frac{4\pi}{3} + \theta\right) + \cos\left(\frac{2\pi}{3} + \theta\right)\right], \\
\omega_{qc,n} &= \omega_{i,n} + g_c^2 \Big/ \left[\cos\left(\frac{6\pi}{3} + \theta\right) + \cos\left(\frac{4\pi}{3} + \theta\right)\right].
\end{aligned}
$$

Generally, the typical qubit level can be modulated in the range of 100 MHz to 15 GHz,[49,50] providing a considerable adjustability in experiment.

Then the effective Hamiltonian becomes

$$
H'_{\text{eff}} = \sum_n [J_1 b_n^\dagger a_n + J_2 c_n^\dagger b_n + J_3 a_{n+1}^\dagger c_n + \text{H.c.}]. \qquad (9)
$$

This shows that the one-dimensional circuit-QED lattice is constructed as a generalized SSH model, the topological phases are characterized by an integer index — the Chern number.[51]

3. Quantum state transfer channel assisted by topological edge states

In this section, we will demonstrate that two-qubit state transfer can be implemented via topologically protected edge states of the effective model in Eq. (9). The wave function of the edge states can be described as

$$|\psi_E(\theta)\rangle = \sum_{n=1} \lambda^n(\theta)(\alpha a_n^\dagger + \beta b_n^\dagger + \gamma c_n^\dagger)|G\rangle, \tag{10}$$

where $|G\rangle = |\,0,\,0,\,0,\,0,\,\ldots,\,0,\,0,\,0,\,0\rangle$. α, β and γ denote the probability amplitudes of the gap state. λ is the localized index. The probability amplitude on resonator n decays (increases) exponentially when $|\lambda| < 1$ ($|\lambda| > 1$), corresponding to the left (right) edge state, if the wave function is normalized.[38,52] Here we take the eigenenergy of an edge state as E. Substituting Eqs. (9) and (10) into Schrödinger equation $H'_{\rm eff}|\psi_E(\theta)\rangle = E|\psi_E(\theta)\rangle$, we can derive the following formulas:

$$\begin{aligned} E\lambda^n(\theta)\alpha a_n^\dagger|G\rangle &= [J_1\alpha\lambda^n(\theta)b_n^\dagger + J_3\alpha\lambda^{n+1}(\theta)c_n^\dagger]|G\rangle, \\ E\lambda^n(\theta)\beta b_n^\dagger|G\rangle &= [J_2\beta\lambda^n(\theta)c_n^\dagger + J_1\beta\lambda^n(\theta)a_n^\dagger]|G\rangle, \\ E\lambda^n(\theta)\gamma c_n^\dagger|G\rangle &= [J_3\gamma\lambda^{n-1}(\theta)a_n^\dagger + J_2\gamma\lambda^n(\theta)b_n^\dagger]|G\rangle. \end{aligned} \tag{11}$$

By calculating, the specific wave function of the topological edge state can be obtained, with

$$|\psi_\pm\rangle = \sum_n \left[\mp\frac{\cos(\frac{4\pi}{3}+\theta)}{\cos\theta}\right]^n \frac{a_n^\dagger \pm b_n^\dagger}{\sqrt{2}}|G\rangle. \tag{12}$$

We can see that the edge states of this lattice only occupy the $a-$ and $b-$ type resonators. When $\theta \in (0,\frac{\pi}{3})\bigcup(\frac{5\pi}{6},\frac{4\pi}{3})$ $[\theta \in (\frac{\pi}{3},\frac{5\pi}{6})\bigcup(\frac{4\pi}{3},\frac{11\pi}{6})]$, the corresponding edge state is concentrated toward the left (right) resonators. Particularly, we also find that the edge state is localized in the two leftmost resonators when $\theta = \pi/6$ or $\theta = 7\pi/6$, and in the two rightmost resonators when $\theta = \pi/2$ or $\theta = 3\pi/2$. Under these circumstances, the two leftmost and rightmost resonators are decoupled from the rest of the lattice. The relevant edge states can be expressed as

$$\begin{aligned} |L\rangle &= \frac{1}{\sqrt{2}}(|10\rangle \pm |01\rangle)_{a_1b_1}|\,0,\,0,\,\ldots,\,0,\,0,\,0,\,0\rangle, \\ |R\rangle &= |\,0,\,0,\,0,\,0,\,\ldots,\,0,\,0\rangle\frac{1}{\sqrt{2}}(|10\rangle \pm |01\rangle)_{a_Nb_N}. \end{aligned} \tag{13}$$

To verify the correctness of the above analysis, we plot the energy spectrum and the state distribution when the size of the lattice is $N = 7$. In Fig. 2(a), there exist one pair of topological edge states labeled as blue and pink. They are separated well from the bulk states. And in Fig. 2(b), we observe that the blue edge state is tend to be localized in the two leftmost resonators when $\theta \in (0,\frac{\pi}{3})\bigcup(\frac{5\pi}{6},\frac{4\pi}{3})$ and in the two rightmost resonators when $\theta \in (\frac{\pi}{3},\frac{5\pi}{6})\bigcup(\frac{4\pi}{3},\frac{11\pi}{6})$. Note that, the gap state has a peculiar distribution in the two leftmost (rightmost) resonators with the approximately same probability. Apparently, the numerical analysis is consistent with the theoretical results. The distribution of the pink gap state is the same as that of the blue gap state. It provides a foretaste that the system can realize the special state transfer between the left state $|L\rangle$ and the right state $|R\rangle$ with θ varying from 0 to 2π. Specially, we take $\theta(t) = \Omega t$, with Ω is the gradient describing the variation rate of θ. So, we can achieve the QST via the evolution of the time-dependent Hamiltonian.

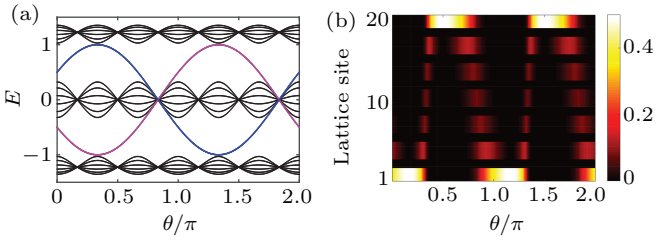


Fig. 2. Energy spectrum and distribution of the edge states when $N = 7$. Here, we take g_j $(j = 1,2,3,a,b,c)$ as the energy unit. (a) Energy spectrum of the system. The lattice has a pair of gap states in the gap. (b) Distribution of the blue edge state. When $\theta \in (0,\frac{\pi}{3})\bigcup(\frac{5\pi}{6},\frac{4\pi}{3})$ $[\theta \in (\frac{\pi}{3},\frac{5\pi}{6})\bigcup(\frac{4\pi}{3},\frac{11\pi}{6})]$, the corresponding edge state is concentrated toward the two leftmost (rightmost) resonators.

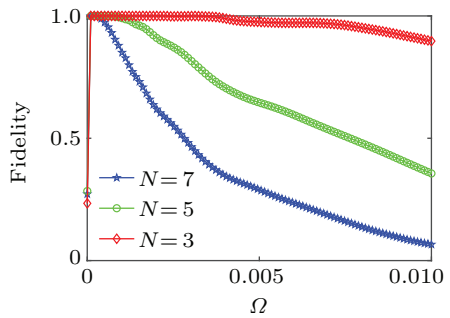


Fig. 3. Fidelity between the right state $|R\rangle$ and the final evolved state versus the varying rate Ω corresponding to different N. Here, we take g_j $(j = 1,2,3,a,b,c)$ as the energy unit.

To access the quality of this QST, we calculate the fidelity of the state transfer from $|L\rangle$ to $|R\rangle$ with the varying of Ω corresponding to different sizes of the lattice. The fidelity is defined as $F = |\langle R|\psi(f)\rangle|$, where $|\psi(f)\rangle$ represents the final state governed by the Schrödinger equation and $|R\rangle$ represents the target state of adiabatic evolution. The simulation results are shown in Fig. 3. We observe that the fidelity $F > 90\%$ can be achieved for $N = 3$. But different lattice lengths with the same Ω will respond differently for the state transfer results. Larger lattice require a smaller Ω to achieve the effective QST. This is because the QST channel is assisted by the edge states of the energy gap and the width of the gap in a generalized SSH model usually exhibits an exponential decay behavior as the system size increases. As a result, corresponding to a large

size of the chain, the varying rate of parameter θ should be small to satisfy the adiabatic condition. While the smaller size of the lattice corresponds to a larger energy gap, which means that Ω can take a relatively larger value (adiabatic condition is easier to satisfy).[47]

In order to further prove that our scheme can be implemented under appropriate adiabatic conditions, we prepare the initial state in $|\Psi_i\rangle = |L\rangle$. The time-dependent state evolution governed by $H'_{\rm eff}(\theta_t)$ corresponding to different lattice sizes is shown in Fig. 4. We choose Ω = 0.0001 for different lattice lengths in Figs. 4(a)–4(c), the images demonstrate that robust two-qubit QST can be realized with the appropriate parameter Ω. By contrast, in Fig. 4(d) we choose $\Omega = 0.01$ and other conditions are consistent with Fig. 4(c), it is straightforward to find that our scheme is completely noneffective.

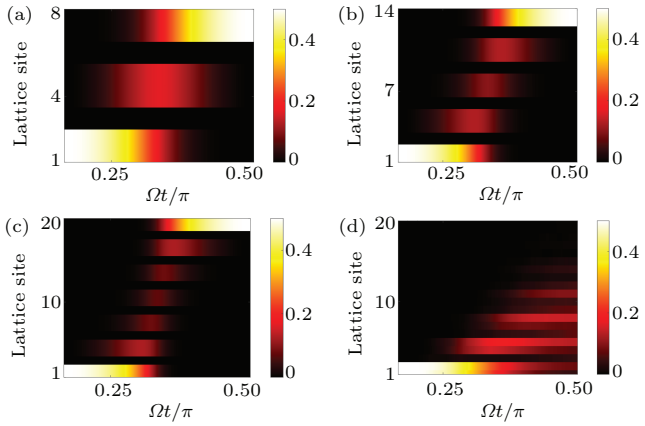


Fig. 4. The time-dependent evolution of the left state $|L\rangle$ to the right state $|R\rangle$ when N takes different values. Here, we take g_j $(j = 1,2,3,a,b,c)$ as the energy unit. (a) $N = 3$ and $\Omega = 0.0001$. (b) $N = 5$ and $\Omega = 0.0001$. (c) $N = 7$ and $\Omega = 0.0001$. (d) $N = 7$ and $\Omega = 0.01$.

4. The defect-induced single-qubit quantum state transfer channel

In Section 3, we have demonstrated that the two-qubit quantum state can be transferred via topological edge states in a 1D circuit-QED lattice. However, in the actual circuit, there are some kinds of random disorder and fluctuations in the physical system. Next, we mainly discuss the fluctuation caused by the on-site defect potential and reveal that it can play an active role in the QST channel. First, we introduce the random on-site defect potential

$$H_{\rm defect} = \Sigma_n W i_n^\dagger i_n, \tag{14}$$

where W represents the strength of defect potential added on the all i-type resonators of the n-th unit cell ($i = a, b$ or c). Under the condition of large enough samples of on-site defect, we numerically simulate the fidelity of the QST scheme with on-site defects corresponding to different-type resonators with random strengths in Fig. 5. From the curve, we can obtain the following two points. Firstly, the efficiency of the scheme decreases with the increase of the strength of the defect added on the a- or b-type resonators. But for the c-type resonators, there is little impact on the high-efficiency QST. Secondly, with the mild defect strength added on the random i-type resonator, our scheme can still be achieved with high fidelity. To summarize, the c-type resonators with on-site defects of relatively high strength are more robust than the a- or b-type resonators in our QST scheme. The reason can be obtained from Eq. (12) in which the edge state occupies only the a- and b-type resonators.

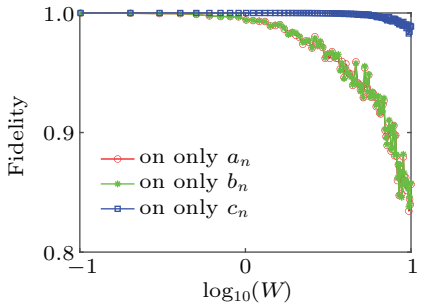


Fig. 5. Fidelity between the right state $|R\rangle$ and the final evolved state versus the strength of random on-site defect added on different resonators. The red circle line represents the random on-site defects added only on the a-type resonators. The green star line represents the random on-site defects added only on the b-type resonators. The blue squre line represents the random on-site defects added only on the c-type resonators. Here, we take g_j $(j = 1,2,3,a,b,c)$ as the energy unit.

In Fig. 5, we obtain that the on-site defect potentials added on a- or b-type resonators randomly have adverse effects on the QST scheme. In the following, we specifically consider the influence on the system when on-site defects with different strengths are added on the first resonator a_1. In this situation, the Hamiltonian of the system can be expressed as

$$\begin{aligned} H_{\rm eff}^{a'} = {} & W a_1^\dagger a_1 + \sum_n \left[\cos\left(\frac{2\pi}{3}+\theta\right) b_n^\dagger a_n \right. \\ & + \cos\left(\frac{4\pi}{3}+\theta\right) c_n^\dagger b_n \\ & \left. + \cos\left(\frac{6\pi}{3}+\theta\right) a_{n+1}^\dagger c_n + \text{H.c.} \right]. \end{aligned} \tag{15}$$

On this basis, we plot the state transfer fidelity as a function of the different on-site defect strength in Fig. 6. We observe that the QST channel maintains good working condition with a high fidelity for $\log_{10}(W) < -0.8$, while the channel is totally ineffective with a zero fidelity corresponding to $\log_{10}(W) > 0$. These results indicate that our work is robust for mild defect strength and a larger defect potential is added on the first resonator can seriously hamper the implementation of the QST scheme.

To figure out the specific impacts of a larger defect potential for the system, we also plot the relevant energy spectrum with different defect strengths in Fig. 7. When $W = 0.1$, Fig. 7(a) shows that the existence of the on-site defect potential makes the energy spectra slightly deform. The reason is that the presence of the mild defects causes a fluctuation in the energy of the system. But we still can notice that there

are two gap states in the energy spectrum. Rather, when the strength $W = 10$, the band structure and the gap states of the system in Fig. 7(b) are quite different from those in Fig. 2(b). Apparently, the band structure and the gap states are changed intensively following the growth of the strength W. That is, a lager defect will steer the first resonator a_1 decoupled from the initial lattice and change the energy spectrum of the initial system completely.

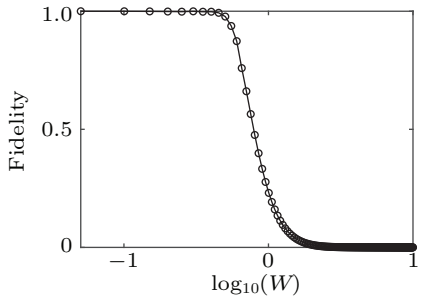


Fig. 6. The effects of the on-site defect added on the first resonator on the system. Fidelity between the right state $|R\rangle$ and the final evolved state versus the strength of on-site defect added on the first resonator. Here, we take g_j $(j = 1,2,3,a,b,c)$ as the energy unit.

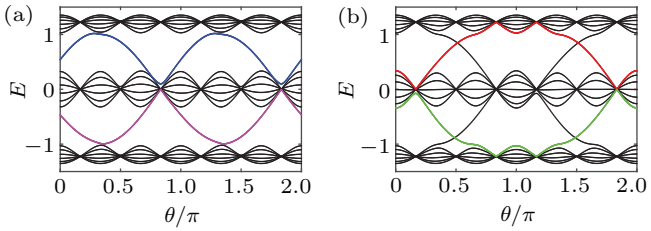


Fig. 7. The effect of the on-site defect added on the first resonator on the system. Here, we take g_j $(j = 1,2,3,a,b,c)$ as the energy unit. (a) Energy spectrum with $W = 0.1$. (b) Energy spectrum with $W = 10$. The unit cells with $N = 7$.

To unambiguously validate that the distribution of edge states can be adjusted accordingly with the on-site defect added on the first resonator, we make a more detailed analysis of the changed energy spectrum in Fig. 8. The state distributions and the corresponding time-dependent evolution of the blue gap state (Fig. 7(a)) are shown in Figs. 8(a) and 8(b). In Fig. 7(a) with $W = 0.1$, the numerical results reveal that the blue gap state exhibits a special distribution, in which it is mainly localized near the first resonator when $\theta = 0.83\pi$ and $\theta = 1.8\pi$ while it is mainly localized at the two leftmost (rightmost) resonators with the same probability at $\theta \in (0, 0.3\pi) \cup (\pi, 1.3\pi)$ ($\theta \in (0.3\pi, 0.8\pi) \cup (1.3\pi, 1.8\pi)$). It means we can achieve a new state transfer $|1\rangle_{a_1}|0,0,0,\ldots,0,0,0,0\rangle \to |L\rangle \to |R\rangle$ as θ varies from 0.83π to 1.5π. If we set the initial state of the system as $|1\rangle_{a_1}|0,0,0,\ldots,0,0,0,0\rangle$, the corresponding process of the state transfer with $H_{\rm eff}^{a'}(\theta_t)$ is shown in Fig. 8(b). This enables us to achieve a simplified two-qubit QST. That is, we can inject a photon in the first resonator and achieve the two-qubit state transfer from $|L\rangle$ to $|R\rangle$. We think this process of preparing a single qubit state, and then evolving to $|L\rangle$ maybe simpler and more convenient than preparing two-qubit entangled states in the first two resonators directly. In Fig. 8(c), the distribution of the edge state for $W = 0.1$ is consistent basically with the initial system under the ideal conditions in Fig. 2(b). This is the reason that the fidelity of state transfer in Fig. 6 is not affected when the defect strength is relatively small. Figure 8(d) is the corresponding evolution of the initial state $|L\rangle$ with time-dependent Hamiltonian $H_{\rm eff}^{a'}(\theta_t)$.

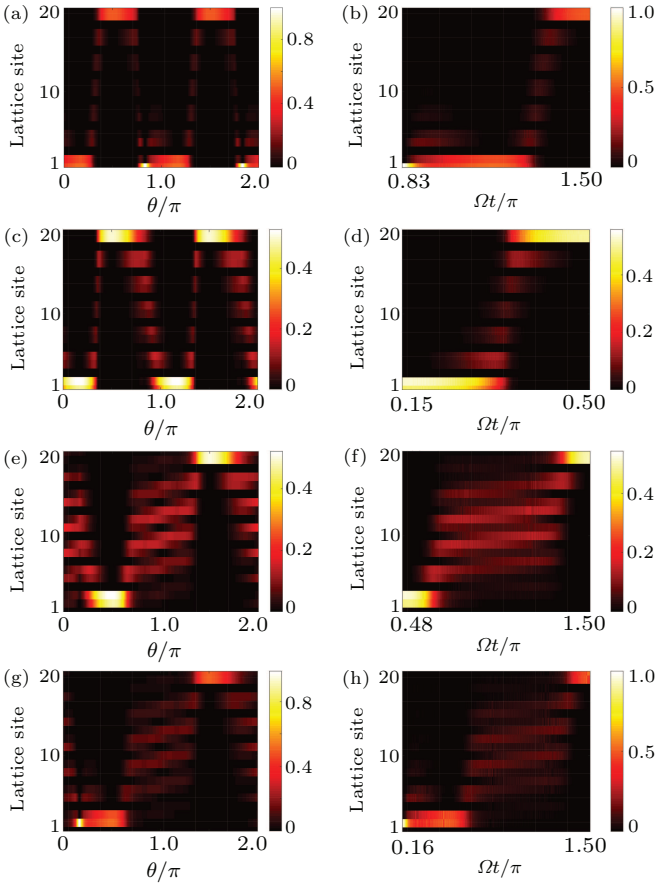


Fig. 8. The effects of the on-site defect added on the first resonator on the system. Here, we take g_j $(j = 1,2,3,a,b,c)$ as the energy unit. (a), (b) The distribution of the blue gap state with $W = 0.1$ and the corresponding time-dependent evolution of the initial state $|1\rangle_{a_1}|0,0,0,\ldots,0,0,0,0\rangle$. (c), (d) The distribution of the pink gap state with $W = 0.1$ and the corresponding time-dependent evolution of the initial state $|L\rangle$. (e), (f) The distribution of the red gap state with $W = 10$ and the corresponding time-dependent evolution of the initial state $\frac{1}{\sqrt{2}}|10 \pm 01\rangle_{b_1c_1}|0,\ldots,0,0,0,0\rangle$. (g), (h) The distribution of the green gap state with $W = 10$ and the corresponding time-dependent evolution of the initial state $|1\rangle_{b_1}|0,0,\ldots,0,0,0,0\rangle$. Other parameters take $N = 7$ and $\Omega = 0.00001$ in (b), (d), (f), and (h).

If considering the greater defect strength with $W = 10$, the distribution and corresponding evolution of the edge states (the red and green gap states in Fig. 7(b)) shown in Figs. 8(e)–8(h) are totally different. Figures 8(e) and 8(f) prove that the red energy gap state can be utilized to construct a new two-qubit QST channel with the new left edge state $|L\rangle_{\rm new} = \frac{1}{\sqrt{2}}|10 \pm 01\rangle_{b_1c_1}|0,\ldots,0,0,0,0\rangle$ to $|R\rangle$. Figures 8(g) and 8(h) indicate that another QST channel with $|1\rangle_{b_1}|0,0,\ldots,0,0,0,0\rangle \to |L\rangle_{\rm new} \to \frac{1}{\sqrt{2}}|0,0,0,\ldots,0,0\rangle|10 \pm 01\rangle_{a_Nb_N}$ is generated.

The above results reveal that the large on-site defect added on the first resonator can make the gap state own dif-

ferent distributions, and the different states transfer between the left- and right-edge states can be achieved. Similar results can be obtained if we consider adding the on-site defect in the last resonator b_N.

Compared with adding a defect on a_1 or b_N in the lattice, we find different interesting phenomenon when the large on-site defect potentials are added on the two ends of the lattice. In this circumstance, the system Hamiltonian manifests as

$$\begin{aligned} H_{\text{eff}}^{ab'} &= (Wa_1^{\dagger}a_1 + Wb_N^{\dagger}b_N) \\ &+ \sum_n \left[\cos\left(\frac{2\pi}{3}+\theta\right) b_n^{\dagger}a_n + \cos\left(\frac{4\pi}{3}+\theta\right) c_n^{\dagger}b_n \right. \\ &\left. + \cos\left(\frac{6\pi}{3}+\theta\right) a_{n+1}^{\dagger}c_n + \text{H.c.} \right]. \end{aligned} \tag{16}$$

Here, we take $W = 10$. When the on-site defects are added on a_1 and b_N, the two end resonators decouple from the initial lattice and the changed energy spectrum is shown in Fig. 9(a), in which the different gap states are drawn in different colors. The state distributions and the corresponding time-dependent evolution of the green and red gap states are shown in Figs. 9(b) and 9(c). Those of the blue and pink gap states are shown in Figs. 9(d) and 9(e). From Fig. 9(b), we can observe that the edge states mainly localize near c_{N-1} and a_N at $\theta \in (0, 0.3\pi) \cup (\pi, 1.3\pi)$ while they appear near b_1 and c_1 at $\theta \in (0.3\pi, 0.6\pi) \cup (1.3\pi, 1.6\pi)$. It means that a new two-qubit state transfer from the initial state $\frac{1}{\sqrt{2}}|0,0,0,\ldots,0\rangle|10 \pm 01\rangle_{c_{N-1}a_N}$ to the final state $\frac{1}{\sqrt{2}}|10 \pm 01\rangle_{b_1c_1}|0,\ldots,0,0,0\rangle$ can be realized. The corresponding process of the state transfer between the new left- and the new right-edge states governed by Eq. (16) is shown in Fig. 9(c). More interestingly, from Fig. 9(d), we can observe that the distribution of the edge state only occupies a separate resonator a_N or b_1. The edge state is concentrated on the second resonator b_1 when $\theta = 0.17\pi$ and $\theta = 1.2\pi$ while it is localized in the penultimate resonator a_N at $\theta = 0.5\pi$ and $\theta = 1.5\pi$. This is different form the case in any of the previous discussions, then it is natural to construct a channel of the single state transfer between the topological new left- and right-edge states. The corresponding evolution of the quantum state from the initial state $|1\rangle_{b_1}|0,0,\ldots,0,0,0\rangle$ to the final state $|0,0,0,\ldots,0,0\rangle|1\rangle_{a_N}$ is shown in Fig. 9(e).

It should be pointed out that a previous research[46] has studied the influence of defects on QST with a superconducting qubit chain. In that work, the QST only occurs along the a-type resonators, so the on-site defects are added on the a-type resonators (the first one and the last one) accordingly. Via designing the on-site defect added on the a-type resonators, a controllable switch mechanism of the QST channel is developed. Different from the former, we here study the on-site defect added on a single i-type resonator ($i = a, b, c$) respectively or different types of resonators simultaneously, to systematically study the influence of the on-site defect on the edge states and QST. And the results here prove that the temperate on-site defects on suitable resonators can change the energy structure and state distribution of the circuit-QED lattice system. These changes drive the conversion of the current system from the two-qubits QST channel to a single-qubit channel. This novel controlling mechanism allows researchers to establish multi-functional QST channels without increasing or decreasing the size of the system.

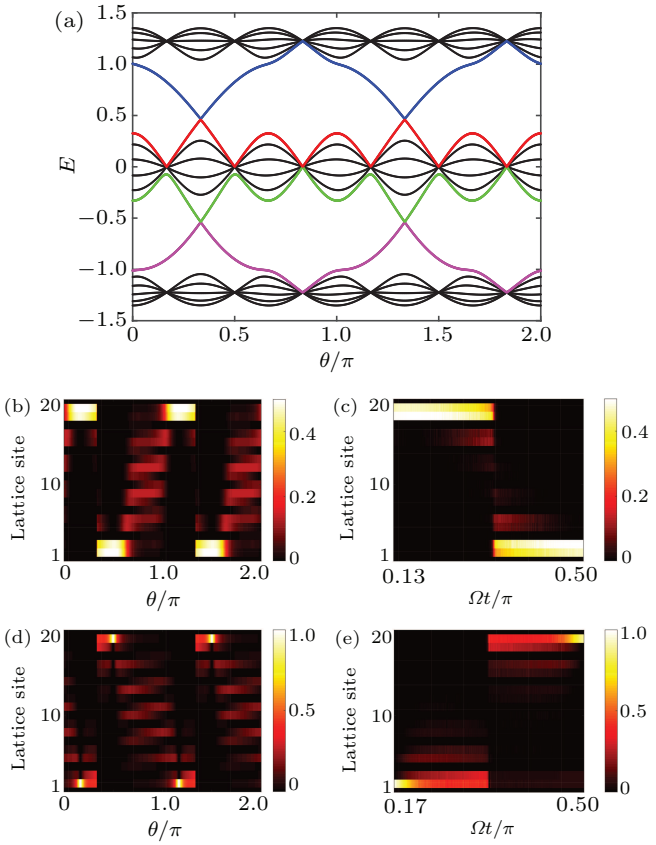


Fig. 9. The effect of the on-site defect added on the two ends of the resonators on the system. Here, we take g_j ($j = 1, 2, 3, a, b, c$) as the energy unit. (a) Energy spectrum with $W = 10$. (b), (c) The distribution of the green (red) gap state and the corresponding time-dependent evolution of the initial state $\frac{1}{\sqrt{2}}|0,0,0,\ldots,0\rangle|10 \pm 01\rangle_{c_{N-1}a_N}$. (d), (e) The distribution of the blue (pink) gap state and the corresponding time-dependent evolution of the initial state $|1\rangle_{b_1}|0,0,\ldots,0,0,0\rangle$. Other parameters take $N = 7$ and $\Omega = 0.00001$ in (c) and (e).

5. Discussion

Before concluding, a feasibility analysis for the schemes involved is necessary. First, the imperfection of experiment equipment and operations may cause $J_k = \cos(\frac{2\pi k}{3} + \theta)$ ($k = 1$, 2, 3) to not be satisfied precisely. Under this circumstance, it is essential to study the influence of non-ideal coupling parameters $J_{\text{n-ideal}} = V\delta + \cos(\frac{2\pi k}{3} + \theta)$ ($k = 1$, 2, 3) on our QST schemes, where δ is a random number in the range of $[-0.5, 0.5]$. Taking the two-qubit QST scheme in Section 3 as an example, we plot the energy spectrum corresponding to the

imperfection coupling parameter with $V = 0.03$ for the system in Fig. 10(a). Note that some slight fluctuations appear in the band structure and the edge states produce tiny oscillations between the energy gap. In Fig. 10(b), when $V = 0.09$, there are two gap states in the the energy spectrum and the edge states produce greater oscillations. However, when the disorder strength exceeds the size of the energy gap, the bulk structure will be broadened and the edge state will blend into the bulk state as shown in Fig. 10(c). It is well known that larger perturbations of edge state will directly affect the effectiveness of QST. So, in Fig. 10(d), we show the fidelity of QST vs. the non-ideal coupling strength V. By the curve, we demonstrate that small fluctuations of coupling strength V will not greatly affect the performance of the scheme.

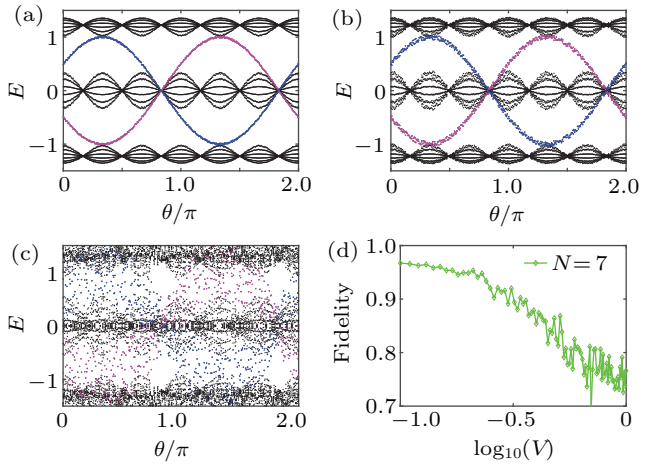


Fig. 10. The effect of non-ideal coupling on the system. Here, we take g_j $(j = 1,2,3,a,b,c)$ as the energy unit. (a) The energy spectrum of the system with $V = 0.03$. (b) The energy spectrum of the system with $V = 0.09$. (c) The energy spectrum of the system with $V = 1.13$. (d) The fidelity of QST vs. the non-ideal coupling strength V and $\Omega = 0.0005$. The unit cells $N = 7$.

Considering a closed Hilbert space, we can realize robust protocols of single-qubit and two-qubit QST theoretically. But, in the actual physical process, the influence of qubits decay and photon leakage out of the transmission line resonators should be considered. The conditional Hamiltonian of an open system for our physical model can be written as[56,57]

$$H = H'_{\text{eff}} - \mathrm{i}\frac{\kappa_{i,n}}{2}\Sigma_n i_n^+ i_n - \mathrm{i}\frac{\gamma_{j,n}}{2}\Sigma_n |e\rangle_{j,n}\langle e|, \tag{17}$$

where H'_{eff} is given by Eq. (9). The second and the third terms represent the photon leakage out of the transmission line resonators and the decay of qubits, respectively. In our protocol, the role of superconducting qubit is to regulate the coupling strength between adjacent resonators, and the generalized SSH model mainly contains the coupling between two nearest-neighbor resonators. So, the photon leakage out of the transmission line resonators is the primary dissipative factor. The qubit spontaneous decay directly affects the coupling strength between adjacent resonators. It may cause $J_k = \cos(\frac{2\pi k}{3} + \theta)$ $(k = 1,2,3)$ to not be satisfied precisely. In Fig. 10, we have already discussed the effect of imperfections on QST. Based on these analyses, we here consider the terms of H'_{eff} and $-\mathrm{i}\frac{\kappa_{i,n}}{2}\Sigma_n i_n^+ i_n$ for an open system. Then, the system Hamiltonian can be written as

$$H_{\text{cond}} = H'_{\text{eff}} - \mathrm{i}\frac{\kappa_{i,n}}{2}\Sigma_n i_n^+ i_n, \quad (i = a,b). \tag{18}$$

Because the edge states occupy a- and b-superconducting resonators, we mainly consider the decay of these two kinds of resonators during the two-qubits QST. For convenience, we take $N = 3$ as an example and assume $\kappa_{i,n} = \kappa$. The fidelity is formulated as $F = \langle R|\rho|R\rangle$, where $|R\rangle = |0,0,0,0,0,0\rangle\frac{1}{\sqrt{2}}(|10\rangle + |01\rangle)_{a_3b_3}$ is the aim state of an ideal system, and the ρ is the final state governed by the conditional Hamiltonian H_{cond}. Figure 11 shows the relationship between the fidelity F and the different decay rate of resonators. As the decay rate of the resonators increases, the fidelities of the open system show a trend of decline. When the parameter Ω is $\Omega = 0.003$, the current QST channel can efficiently transfer the two-qubits state with 0.99 fidelity under considering the decay of the resonators. For $\Omega = 0.001$, the QST fidelity keeps 0.99 for $\kappa/g \in (0.01, 0.03)$. However, when $\kappa/g \in (0.03, 0.05)$, the fidelity decreases rapidly compared to the other two lines. The reason is that the appropriate adiabatic parameter Ω ensuring the current scheme is protected by the topological gap, but smaller adiabatic parameter means longer evolution time, which leads to a decrease in the effectiveness of the QST scheme in an open system with larger dissipation. Therefore, in an open system, the reasonable choice of adiabatic parameter Ω is helpful to improve the fidelity of the QST scheme.

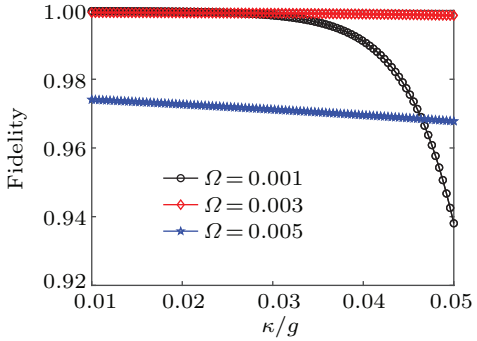


Fig. 11. The fidelity of the QST of $|L\rangle \to |R\rangle$ under the different decay rate κ of resonators when $N = 3$. Here, we take g_j $(j = 1,2,3,a,b,c)$ as the energy unit.

In addition, taking the characteristic of the adiabatic passage, we estimate the QST time of single-qubit (T_1) and two-qubit states (T_2). For the sake of discussion, we set the coupling strength g_j $(j = 1,2,3,a,b,c)$ between the TRL and the flux qubit to 1 as the energy unit. For $N = 7$ and $\Omega = 0.00001$, with the strong coupling strength $g_{j,n}/2\pi = 636$ MHz,[53] the operation times of $T_1 = (0.5\pi - 0.17\pi)/\Omega \approx 25.9$ μs and

$T_2 = (0.5\pi - 0.16\pi)/\Omega \approx 26.2$ μs are both less than the decoherence time of a superconducting coplanar-transmission-line resonator. The lifetime of single microwave photon in superconducting coplanar-transmission-line resonator can reach 0.1 ms.[54,55] Therefore, our schemes can utilize the circuit-QED system such as coplanar resonators and qubits to realize under the development of the current technology, or in the near future. Moreover, the large coupling g_i with the condition $g_i/\Delta_i \ll 1$ is realizable under current experimental conditions. Generally, the typical qubit level can be modulated in the range of 100 MHz to 15 GHz, providing a considerable adjustability in experiment. For $g/2\pi \approx 600$ MHz, the ratio of g_i/Δ_i can be achieved at the highest 600 MHz/15 GHz≈ 0.04. In addition, we might be able to take advantage of the rapid development of fast QST methods, such as introducing the next-to-nearest-neighbor interactions of lattices to cancel nonadiabatic excitations[58] or constructing an exponential time-driving function to vary interchain couplings.[59,60] These methods can satisfy the adiabatic conditions under the premise of shorter time of QST. Therefore, it is of great potential to use accelerated adiabatic process in our model for reducing the coupling strength requirements and improving the feasibility of our schemes.

6. Conclusion

We have realized robust QST schemes based on a 1D circuit-QED lattice. After mapping the system into a generalized SSH model, the QST between the two leftmost resonators and the two rightmost resonators can be realized. We also investigate the influence of the on-site defect added on specific resonators on the QST. Remarkably, a change-over switch mechanism of the QST channel is developed via designing the on-site defect added on the first and the last resonators. In other word, when the on-site defects are added on the two ends of this lattice, a single-qubit state transfer channel is generated. Our work opens up a new way for the realization of topological quantum information processing and provides a path toward the different types of QST via adding the on-site defect on the resonator.

Acknowledgements

This work is supported by the National Natural Science Foundation of China (Grant Nos. 61801280, 61805134, and 61822114), the Applied Fundamental Research Projects of Shanxi Province, China (Grant No. 201801D221015), and Science and Technology Innovation Project of Shanxi Normal University (Grant No. 2020XSY032).

Appendix A: The time-evolve of a 8-resonator lattice chain

The Hamiltonian given in Eq. (9) is described as

$$H'_{\rm eff} = \sum_n [J_1 b_n^\dagger a_n + J_2 c_n^\dagger b_n + J_3 a_{n+1}^\dagger c_n + {\rm H.c.}]$$

where $J_1 = \cos(\frac{2\pi}{3} + \theta)$, $J_2 = \cos(\frac{4\pi}{3} + \theta)$ and $J_3 = \cos(\frac{6\pi}{3} + \theta)$. As a result, we obtain the Schrödinger equation as

$$\mathrm{i}\frac{\partial}{\partial t}\begin{pmatrix} a_1 \\ b_1 \\ c_1 \\ a_2 \\ b_2 \\ c_2 \\ a_3 \\ b_3 \end{pmatrix} = \begin{pmatrix} 0 & J_1(\theta) & 0 & 0 & 0 & 0 & 0 & 0 \\ J_1(\theta) & 0 & J_2(\theta) & 0 & 0 & 0 & 0 & 0 \\ 0 & J_2(\theta) & 0 & J_3(\theta) & 0 & 0 & 0 & 0 \\ 0 & 0 & J_3(\theta) & 0 & J_1(\theta) & 0 & 0 & 0 \\ 0 & 0 & 0 & J_1(\theta) & 0 & J_2(\theta) & 0 & 0 \\ 0 & 0 & 0 & 0 & J_2(\theta) & 0 & J_3(\theta) & 0 \\ 0 & 0 & 0 & 0 & 0 & J_3(\theta) & 0 & J_1(\theta) \\ 0 & 0 & 0 & 0 & 0 & 0 & J_1(\theta) & 0 \end{pmatrix} \begin{pmatrix} a_1 \\ b_1 \\ c_1 \\ a_2 \\ b_2 \\ c_2 \\ a_3 \\ b_3 \end{pmatrix}.$$

According to this equation, first of all, we establish a system of differential equations based on the generalized SSH model. Then, for the initial state

$$|L\rangle = \left(\frac{1}{\sqrt{2}}\ \frac{1}{\sqrt{2}}\ 0\ 0\ 0\ 0\ 0\ 0\right)^{\rm T},$$

we choose the appropriate adiabatic evolution parameter Ω, and the state of the system can be evolved from the time-dependent Schrödinger equation with

$$\mathrm{i}\frac{\partial}{\partial t}\begin{pmatrix} a_1 \\ b_1 \\ c_1 \\ a_2 \\ b_2 \\ c_2 \\ a_3 \\ b_3 \end{pmatrix} = \begin{pmatrix} 0 & J_1(\Omega t) & 0 & 0 & 0 & 0 & 0 & 0 \\ J_1(\Omega t) & 0 & J_2(\Omega t) & 0 & 0 & 0 & 0 & 0 \\ 0 & J_2(\Omega t) & 0 & J_3(\Omega t) & 0 & 0 & 0 & 0 \\ 0 & 0 & J_3(\Omega t) & 0 & J_1(\Omega t) & 0 & 0 & 0 \\ 0 & 0 & 0 & J_1(\Omega t) & 0 & J_2(\Omega t) & 0 & 0 \\ 0 & 0 & 0 & 0 & J_2(\Omega t) & 0 & J_3(\Omega t) & 0 \\ 0 & 0 & 0 & 0 & 0 & J_3(\Omega t) & 0 & J_1(\Omega t) \\ 0 & 0 & 0 & 0 & 0 & 0 & J_1(\Omega t) & 0 \end{pmatrix} \begin{pmatrix} a_1 \\ b_1 \\ c_1 \\ a_2 \\ b_2 \\ c_2 \\ a_3 \\ b_3 \end{pmatrix},$$

where $J_1(\Omega t) = \cos(\frac{2\pi}{3} + \Omega t)$, $J_2(\Omega t) = \cos(\frac{4\pi}{3} + \Omega t)$ and $J_3(\Omega t) = \cos(\frac{6\pi}{3} + \Omega t)$.

More specifically, from Figs. 2 and 4, we can get that the edge state is localized in the two leftmost resonators when $\theta = \pi/6$ or $\theta = 7\pi/6$, and in the two rightmost resonators when $\theta = \pi/2$ or $\theta = 3\pi/2$. Here, we only demonstrate a single direction of evolution when $\theta \in (0, \pi/2)$. In the range of $\theta \in (0, \pi/2)$, the edge state is localized in the two leftmost (rightmost) resonators when $\theta = \pi/6$ ($\theta = \pi/2$)). Therefore, according to $\theta = \Omega t$, the initial time and end time can be expressed as $t_{\text{initial}} = \frac{1}{6\Omega}$ and $t_{\text{end}} = \frac{1}{2\Omega}$. Substituting the relevant parameters of $\Omega = 0.0001$, $|L\rangle$, $t_{\text{initial}} = \frac{1}{6\Omega}$ and $t_{\text{end}} = \frac{1}{2\Omega}$ into the time-dependent Schrödinger equation, we can get the evolution of $|L\rangle$ as shown in Fig. 4. The evolution of all size lattices with N is consistent with this process.

References

[1] Zhu S L, Wang Z D and Yang K Y 2003 *Phys. Rev. A* **68** 034303
[2] Chaneli'ere T, Matsukevich D N, Jenkins S D, *et al.* 2006 *Nature* **438** 833
[3] Cheng S T, Wang C Y and Tao M H 2005 *IEEE J. Sel. Areas Commun.* **23** 1424
[4] Gisin N and Thew R 2007 *Nat. Photon.* **1** 165
[5] Chapuran T E, Toliver P, Peters N A, *et al.* 2009 *New J. Phys.* **11** 105001
[6] Peev M, Pacher C, Alléaume R, *et al.* 2009 *New J. Phys.* **11** 075001
[7] Axline C J, Burkhart L D, Pfaff W, *et al.* 2018 *Nat. Phys.* **14** 705
[8] Cirac J I, Zoller P, Kimble H J and Mabuchi H 1997 *Phys. Rev. Lett.* **78** 3221
[9] Parkins A S and Kimble H J 1999 *J. Opt. B* **1** 496
[10] Van Enk S J, Cirac J I and Zoller P, Kimble H J and Mabuchi H 1997 *J. Mod. Opt.* **44** 1727
[11] Kozhekin A E, Mϕlmer K and Polzik E 2000 *Phys. Rev. A* **62** 033809
[12] Christandl M, Datta N, Ekert A and Landahl A J 2004 *Phys. Rev. Lett.* **92** 187902
[13] de Moraes Neto G D, Andrade F M, Montenegro and Bose S 2016 *Phys. Rev. A* **93** 062339
[14] Jahne K, Yurke B and Gavish U 2007 *Phys. Rev. A* **75** 010301
[15] Yin Z Q and Li F L 2007 *Phys. Rev. A* **75** 012324
[16] Yang W L, Yin Z Q and Xu Z Y, Feng M and Oh C H 2011 *Phys. Rev. A* **84** 043849
[17] Wang Y D and Clerk A A 2012 *Phys. Rev. Lett.* **108** 153603
[18] Stute A, Casabone B, Brandstätter B, *et al.* 2013 *Nat. Photon.* **7** 219
[19] Paternostro M, Palma G M, Kim M S and Falci G 2005 *Phys. Rev. A* **71** 042311
[20] He Q L, Sun J, Song X S and Xiao Y J 2021 *Chin. Phys. B* **30** 010305
[21] Srinivasan S J, Hoffman A J, Gambetta J M and Houck A A 2011 *Phys. Rev. Lett.* **106** 083601
[22] Wallraff A, Schuster D I, Blais A, Frunzio L, Huang R S, Majer J, Kumar S, Girvin S M and Schoelkopf R J 2004 *Nature* **431** 162
[23] Sebastian S and Jens K 2013 *Ann Phys.* **525** 395
[24] Xiang Z L, Ashhab S, You J Q and Nori F 2013 *Rev. Mod. Phys.* **85** 623
[25] Blais A, Huang R S, Wallra A, Girvin S M and Schoelkopf R J 2004 *Phys. Rev. A* **69** 062320
[26] Gu X, Kockum A F, Miranowicz A, Liu Y X and Nori F 2017 *Phys. Rep.* **718–719** 1
[27] Kane C L and Mele E J 2005 *Phys. Rev. Lett.* **95** 226801
[28] Fu L, Kane C L and Mele E J 2007 *Phys. Rev. Lett.* **98** 106803
[29] Hasan M Z and Kane C L 2010 *Rev. Mod. Phys.* **82** 3045
[30] Qi X L and Zhang S C 2011 *Rev. Mod. Phys.* **83** 1057
[31] Chiu C K, Teo J C Y, Schnyder A P and Ryu S 2016 *Rev. Mod. Phys.* **88** 035005
[32] Bansil A, Lin H and Das T 2016 *Rev. Mod. Phys.* **88** 021004
[33] Bonderson P and Nayak C 2013 *Phys. Rev. B* **87** 195451
[34] Paananen T and Dahm T 2013 *Phys. Rev. B* **87** 195447
[35] Yong J, Jiang Y P, Usanmaz D, Curtarolo S, Zhang X H, Li L Z, Pan X Q, Shin J, Takeuchi I and Greene R L 2014 *Appl. Phys. Lett.* **105** 222403
[36] Chazal F, Fasy B, Lecci F, Michel B, Rinaldo A and Wasserman L 2018 *The Journal of Machine Learning Research* **18** 1
[37] Takagaki Y, Giussani A, Perumal K, Calarco R and Friedland K J 2012 *Phys. Rev. B* **86** 125137
[38] Mei F, Chen G, Tian L, Zhu S L and Jia S T 2018 *Phys. Rev. A* **98** 012331
[39] Ribeiro Jr L A, Cunha W F da and Fonseca A L d A, Silva G M and Stafström S 2015 *J. Phys. Chem. Lett.* **6** 510
[40] Qi L, Liu S, Zhang S and Wang H F 2020 *Opt. Lett.* **45** 2018
[41] Alicea J, Oreg Y, Refael G, Oppen F V and Fisher M P A 2011 *Nat. Phys.* **7** 412
[42] Duclos-Cianci G and Poulin D 2010 *Phys. Rev. Lett.* **104** 050504
[43] Bonderson P and Lutchyn R M 2011 *Phys. Rev. Lett.* **106** 130505
[44] Kim I H 2013 *Phys. Rev. Lett.* **111** 080503
[45] Longhi S, Giorgi G L and Zambrini R 2019 *Adv. Quantum Technol.* **2** 1800090
[46] Lemonde M A, Peano V, Rabl P and Angelakis D G 2019 *New J. Phys.* **21** 113030
[47] Zheng L N, Qi L and Cheng L Y, Wang H F and Zhang S 2020 *Phys. Rev. A* **102** 012606
[48] Mei F, Xue Z Y, Zhang D W, Tian L, Lee C H and Zhu S L 2016 *Quantum Sci. Technol.* **1** 015006
[49] Manucharyan V E, Koch J, Glazman L I and Devoret M H 2009 *Science* **326** 113
[50] Manucharyan V E, Masluk N A, Kamal A, Koch J, Glazman L I and Devoret M H 2012 *Phys. Rev. B* **85** 024521
[51] Kraus Y E and Zilberberg O 2012 *Phys. Rev. Lett.* **109** 116404
[52] Qi L, Wang G L, Liu S, Zhang S and Wang H F 2020 *Phys. Rev. A* **102** 022404
[53] Niemczyk T, Deppe F, Huebl H, Menzel E P, Hocke F, Schwarz M J, Garcia-Ripoll J J, Zueco D, Hümmer T, Solano E, Marx A and Gross R 2010 *Nat. Phys.* **6** 772
[54] Vissers M R, Kline J S and Gao J, Wisbeyb S and Pappasc P D 2012 *Appl. Phys. Lett.* **100** 082602
[55] Bruno A, Lange G D, Asaad S, van der Enden K L, Langford N K and DiCarlo L 2015 *Appl. Phys. Lett.* **106** 182601
[56] Pachos J and Walther H 2002 *Phys. Rev. Lett.* **89** 187903
[57] Huang X R, Ding Z X, Hu C S, Shen L T, Li W, Wu H and Zheng S B 2018 *Phys. Rev. A* **98** 052324
[58] D'Angelis F M, Pinheiro F A, Guéry-Odelin D, Longhi S and Impens F 2020 *Phys. Rev. Research* **2** 033475
[59] Huang B H, Kang Y H, Chen Y H, Shi Z C, Song J and Xia Y 2018 *Phys. Rev. A* **97** 012333
[60] Palaiodimopoulos N E, Brouzos I, Diakonos F K and Theocharis G 2021 *Phys. Rev. A* **103** 052409